Chemistry and Biochemistry   College of Arts and Sciences

Summer 7-19-2023

A molten salt test loop for component and instrumentation testing

T L. Head
Abilene Christian University

Allison M. Berry

Keaton J. Brewster

Robert L. Brown

Hailey N. Burden

See next page for additional authors

Recommended Citation

Authors

T L. Head, Allison M. Berry, Keaton J. Brewster, Robert L. Brown, Hailey N. Burden, Reuben Byrd, Timothy Doty, Jess Dowdy, Kameron A. Hill, R. A. Jinkerson, Timothy J. Kennedy, Ronald C. Laehn, Dakotah Martinez, Samuel L. Mulder, Charles Onstead, Kim L. Pamplin, Dylan C. Pfeifer, Michael B. Ranger, Aaron D. Robison, Nathaniel T. Rowlands, Raymond E. Smith, Matthew T. Steele, R. S. Towell, Travis Towell, Olive Tuyishimire, and T. S. Watson

Contents lists available at ScienceDirect

Annals of Nuclear Energy

journal homepage: www.elsevier.com/locate/anucene
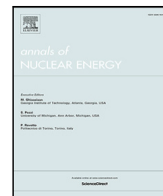
A molten salt test loop for component and instrumentation testing

T.L. Head *, Allison M. Berry, Keaton J. Brewster, Robert L. Brown, Hailey N. Burden,
Reuben Byrd, Timothy Doty, Jess Dowdy, Kameron A. Hill, R.A. Jinkerson, Timothy J. Kennedy,
Ronald C. Laehn, Dakotah Martinez, Samuel L. Mulder, Charles Onstead, Kim L. Pamplin,
Dylan C. Pfeifer, Michael B. Ranger, Aaron D. Robison, Nathaniel T. Rowlands,
Raymond E. Smith, Matthew T. Steele, R.S. Towell, Travis Towell, Olive Tuyishimire,
T.S. Watson

Abilene Christian University, Abilene, 79699, TX, United States

ARTICLE INFO

ABSTRACT

Molten salt is an effective coolant for a wide range of applications, including nuclear reactors, concentrated solar power, and other high temperature industrial heat transfer processes. The technical readiness level of components and instrumentation for high-temperature molten salt applications needs improvement for molten salt to be more widely adopted. A molten salt test loop was designed, built, and commissioned as a test bed to address these issues. The molten salt test loop at Abilene Christian University was built out of 316 stainless steel with a forced flow centrifugal-type pump, and was instrumented for remote operation. A low-temperature molten nitrate salt was used in this system, which was designed to operate at temperatures up to 300 °C and flow rates up to 90 liters per minute.

This paper describes the loop design, computational fluid dynamics modeling, construction, and commissioning details. An outline of the data acquisition and control systems is presented. Salt samples were taken before and after introduction into the loop, and melting points were measured both before and after salt circulation. Performance of the system is discussed as well as improvements required for higher temperature loops envisioned for the future.

1. Introduction

Global interest in clean, efficient, safe, and reliable energy production has led to renewed interest in advanced reactor designs. Nuclear reactors are the only carbon-free energy source that is able to produce electricity on demand. Advanced reactors share the advantages of current commercial reactor technologies while improving in key areas such as safety and minimizing waste generation (Sohal et al., 2010; Worrall et al., 2018).

Molten salt reactors (MSRs) constitute one category of advanced reactors and use molten salt as the reactor coolant. Using molten salt as the heat-transfer fluid from the reactor core to the heat exchanger has potential to improve the reactor safety and efficiency while lowering the cost to produce electricity. These benefits are a direct result of the physical properties of salts in a liquid form (Forsberg et al., 2007). Molten salts have high heat capacities, extremely high boiling points, and low vapor pressures (Jerden, 2019; Williams et al., 2006). The high boiling point ensures that the liquid will never undergo the phase transition to a gas during operation. Therefore, these reactors can operate at

high temperatures (improving efficiency) and low pressure (increasing safety while decreasing costs). Typical operating temperature for a fluoride-based eutectic-salt mixture is between 500 and 700 °C and is based on the maximum temperature of salt-wetted materials rather than on system pressure rating. Operating at these high temperatures means that MSRs can provide high-temperature process heat for many industrial processes including desalination of water, the production of synthetic fuels, and the generation of clean hydrogen (Forsberg, 2006; Ho et al., 2019).

A subset of MSRs also use fuel in a salt form that can be added to the molten salt coolant. These liquid-fueled MSRs have the added advantage of utilizing virtually all of the fissile material in the core and therefore decreasing the radioactive waste being generated (Engel et al., 1978; Rosenthal et al., 1970; Zhang et al., 2018). Liquid-fueled reactors also produce isotopes in the liquid salt, where they can be collected for useful purposes, including medical use. This source of life-saving medical isotopes will provide the medical community with

---

powerful diagnosis and new treatment options for many forms of cancer (Kratochwil et al., 2017; Stoddard et al., 2019; Zheng et al., 2018).

Initial interest in MSRs began at Oak Ridge National Lab in the 1950s and 1960s, leading to the Molten Salt Reactor Experiment (MSRE). The MSRE successfully operated a thermal-spectrum liquid-fueled molten salt reactor for four years with both ^{235}U and ^{233}U as the fuel (None, 1972). The MSRE was a demonstration that was meant to move the molten-salt-based reactor program toward breeder reactors that could breed fertile thorium into fissile ^{233}U. Although a design was under way, the program was terminated before such a reactor could be constructed (MacPherson, 1985).

Recent interest in MSRs has led to the development of a variety of molten salt test systems to help advance the technical readiness level of the many components and instruments needed for the licensing of an MSR. Some operating salt loops with various salt types, including eutectic mixtures of LiF-BeF$_2$ (FLiBe) (Britsch et al., 2019), LiF-NaF-KF (FLiNaK) (Yoder Jr. et al., 2014; Arora et al., 2021; Sabharwall et al., 2010; Ludwig et al., 2011), chloride (Robb et al., 2019; Kelleher et al., 2022; Jeong et al., 2018), and nitrate salts (Gill et al., 2014; Sabharwall et al., 2010) exist at public and private institutions. The Molten Salt Test Loop (MSTL) facility has been built in the Nuclear Energy eXperimental Testing (NEXT) Lab at Abilene Christian University (ACU) to serve as a test bed for MSR technologies, particularly in the areas of instrumentation, reactor component development, and online monitoring of salt and system chemistry.

2. High-level system requirements

The MSTL was designed, built, and commissioned to support a wide range of early research and development needs of the NEXT Lab to advance its mission *to provide global solutions to the world's need for energy, water and medical isotopes by advancing the technology of molten salt reactors while educating future leaders in nuclear science and engineering* (Towell, 2018).

These needs include:

- To provide early design exploration
- To develop salt sampling methods
- To evaluate a fully remote monitoring and control system
- To provide a test bed for novel instrumentation
- To enable student research participation
- To evaluate pump, flange, and other system component performance

A set of high-level system requirements for the MSTL were developed to meet the research and development needs. These system requirements were:

- Store, melt, and circulate salt
- Use materials readily available and capable of ensuring safe operations
- Minimize hazards of all types
- Provide test opportunities for instruments, components, and controls
- Utilize previously procured pump and heating system.

To meet these high-level system requirements decisions such as salt selection, operating temperature, materials selection and system layout had to be made. These decisions were made considering many constraints that are significantly different from those for a reactor including, cost, schedule, hazards present, flexibility and material availability. To meet the high-level system requirements while considering these factors, we made design decisions and developed the following design criteria:

- The working salt will be a eutectic mixture of KNO$_3$-LiNO$_3$-NaNO$_3$ commercially available as Dynalene MS-2 (Dynalene, 2020).
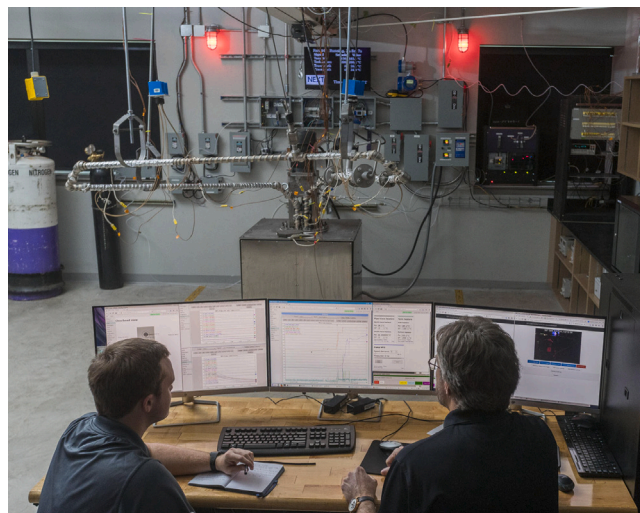

Fig. 1. The MSTL during trace heating tests before insulation is applied to the loop. The box at the bottom contains the sump tank, heaters, and insulation for the tank. The pump sits atop the sump. Piping is wrapped with heat tape and, in some places, with foil to spread the heat.

- The system will hold at least 17 L of liquid salt.
- The system will be able to operate up to 300 °C.
- The system will be constructed from 316 stainless steel.
- The system will be capable of flow rates from 14 to 70 L/min.
- The system will have a nitrogen cover gas system.
- The system will provide means of salt and cover gas sampling.
- The system will be remotely operated and monitored.
- The system will be equipped with instrumentation beyond the minimum control requirements.

The design of the MSTL was completed in 2017, and the first circulation of molten salt was successfully completed on October 23, 2018.

The following sections describe the overall design, major system components, initialization and testing of the system (shown in Fig. 1), analysis of the salt, and changes that will be required for more advanced systems.

3. Major system components

The MSTL was assembled and installed in Bennett Lab at ACU, where 3-phase power for the pump and heaters is available as well as appropriate room ventilation and a vent for cover gas exhaust. The system consists of a centrifugal sump-type pump system, a 316 stainless steel salt container, a 316 stainless steel salt loop (Fig. 2), a cover gas system, heaters for the salt container, trace heating for the loop pipes, and a data acquisition and control system. This section will describe each of these systems in detail.

The concept of system operation is to melt the salt in the sump tank by setting the temperature significantly above the salt melting temperature, then heat the loop to above the melting point using trace heaters, then start the pump once the loop is heated. When the pump reaches a rotational speed high enough to develop the pressure required for the salt to reach the apex of the loop, salt flows through the loop and back into the sump tank, where it can start around the loop again. After flow through the loop is completed and the pump is turned off, salt is drained from the loop into the sump tank by inserting gas at the top of the loop.
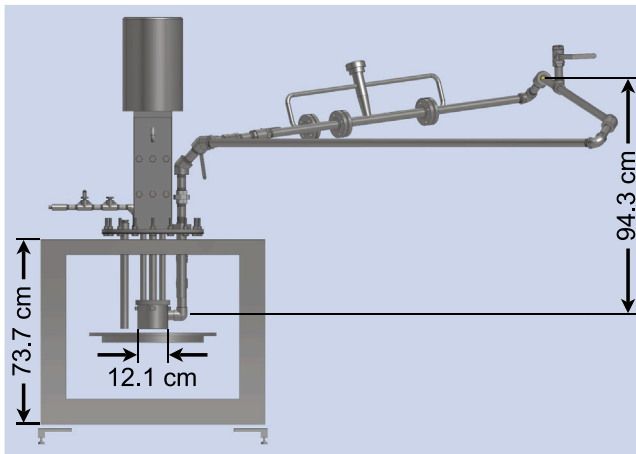
Fig. 2. A rendered perspective view of the MSTL showing the triangular loop configuration with the pump motor shown atop the pedestal, flow meter shown along the loop at the top of the image, and the tee and valve used for pressure equalization near the high point of the loop. The figure shows the distance from the center of the pump outlet to the center of the pipe at the high point of the loop, the height of the pedestal containing heaters and insulation and the width of the volute which houses the impeller.

Fig. 3. The flange of the MSTL, on top of which the pump was mounted. The two rectangular structures centered top and bottom are supports for the pump bearings and motor. Two 25 mm diameter experimental ports are located to the right of the shaft and are shown capped. The upper port, labeled sampling port, has a pipe that goes down near the bottom of the sump. The lower port terminates at the bottom face of the flange and is reduced and used as a gas outlet.

3.1. Pump

The molten salt pump is a centrifugal-style pump made of all 316 stainless steel construction mounted to a circular flange 12.5 mm thick and sealed with a calcium silicate gasket. The flange layout is shown in figure Fig. 3. The pump is powered by a 2.2 kW motor connected to the 73.5 cm long pump shaft by a chain coupling. The 37.5 mm diameter pump shaft is mounted axial with the motor. The pump shaft bearings and supports are in air at temperatures less than 200 °C and are not salt-wetted. The pump shaft penetrates the sump through a packing gland packed with graphite-impregnated fiberglass. Where the pump shaft penetrates the volute that houses the impeller, there is a small gap where some salt leaks out when the pump is running. The pump supplies up to 90 L/min of flow through the system with motor rotation rates up to 3600 RPM by drawing molten salt from a sump through a 25 mm diameter inlet at the bottom of the volute and discharging the salt through a 25 mm diameter pipe. The impeller shown in Fig. 4 has two blades and a diameter of 8.3 cm. The manufacturer was unable to supply a pump curve for the system.

3.2. Sump tank and heaters

The Dynalene MS-2 salt for the system resides in the sump tank (Fig. 5), in which the pump is suspended. The tank has a 33.0 cm inside diameter and a 38.1 cm interior depth. The tank holds 19 L of liquid salt with 7.5 L of gas headspace. The sump in this design is integrated with the top plate of a heater box and mates with the pump using a flat insulating gasket and 17 equally spaced 0.95 mm threaded studs welded to the top of the sump. A nominal seal between the pump flange and the sump is provided by calcium silicate insulating paper. The sump tank is heated in two zones: the side of the tank and below the tank. The side heaters are vacuum-formed ceramic heaters with wound NiCr wire elements. The bottom heater is a calrod-type heater similar to a stove element. Together, the side and bottom heaters supply up to 11 kW of power to the sump. The elements are independently controllable so that during remelting, the salt can be heated from the top so as not to deform the sump tank due to thermal expansion of the lower salt sealed by a solid top plug.
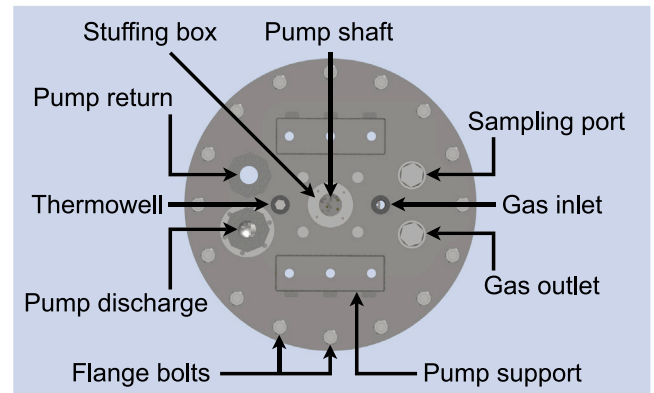

Fig. 4. MSTL pump impeller. The impeller is made of 316 stainless steel. The scale numbers are in cm.

3.3. Salt loop

The salt loop consists of 7.8 m of 25 mm schedule 40, 316 stainless steel pipe. The pipe is fitted in a semi-triangular design for ease of assembly, see Fig. 2, with the pipe pieces connected using NPT fittings and polytetrafluoroethylene (PTFE) tape required to help reduce friction enough to seal the joints. NPT fittings were initially used to match the fittings provided by the pump manufacturer and to reduce cost with a plan to weld the fittings if leakage became a problem. The joints sealed so that welding was not necessary, and provided more flexibility to change the system as needed in the future. The PTFE tape (melting point 327 °C Christakopoulos et al., 2020) is the
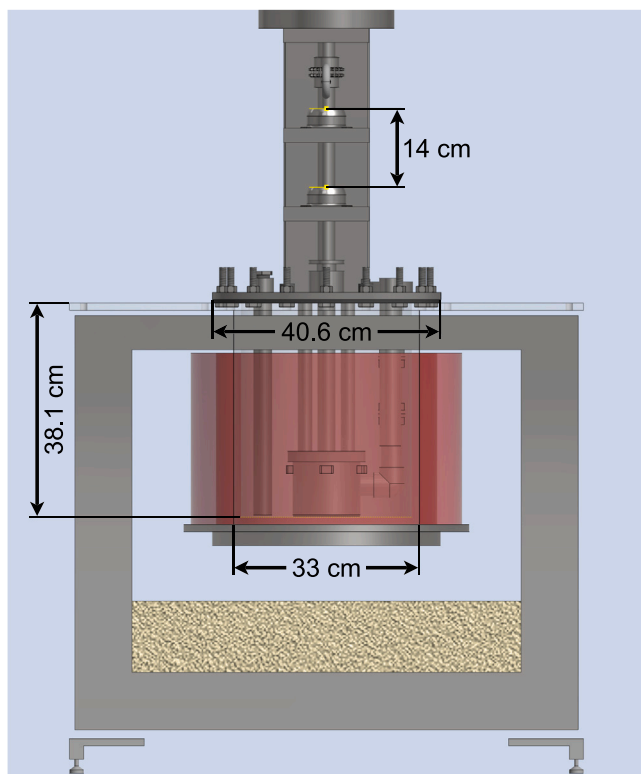
Fig. 5. Rendered cross section of the MSTL salt pump and sump tank region showing the volute and pump structural supports surrounded by the sump tank. The measurement shows the diameter and height of the sump tank, the diameter of the pump mounting flange, and the spacing between bearings for the pump shaft.

limiting factor in the temperature rating of the system. Other higher-temperature sealants and lubricants were tried unsuccessfully to help seal the threaded connections. The pump discharges molten salt directly into the loop, and the salt then goes past a tee that is valved off, through a 25 mm diameter stainless steel valve, and then travels up through an ultrasonic flow meter. The flowmeter is a Krohne Optisonic model 4400HT with pipe size 25 mm, and the maximum temperature for process fluid limited to 400 °C. Continuing around a corner to the high point of the loop, there is another tee. This tee is placed vertically with gas space and a gas supply to allow for both salt expansion and with the appropriate gas control to allow salt to drain back into the sump. The salt then flows downhill around another corner to the salt-return to the sump. The loop return into the sump is an open pipe set at the height of the top of the pump volute. The salt-return goes into the sump below the salt surface level to avoid creating excess bubbles in the system. The total elevation change of the system from the pump discharge is 94.3 cm.

The loop is supported by pipe hangers to reduce stress on the piping. The pipe hangers are insulated from the pipe with calcium silicate paper insulation to reduce the thermal transfer to the support while avoiding insulation compression. The bulk of the loop is insulated with an additional fiberglass layer and is covered with 22.9 cm diameter galvanized steel sheet.

3.4. Cover-gas system

Corrosion minimization for the loop is accomplished in large part by the cover gas system. When not actively pumping, the system maintains a nitrogen blanket throughout the loop and above the salt sump. The system was not designed to be gas tight, and so has a significant leak rate. A flow rate of 1 to 1.5 L/min of dry nitrogen at room temperature is provided to the system to ensure that it stays as dry as possible.

Additionally, the cover gas system is used to provide cover gas to the high point in the loop so that, with proper pressure control, salt can flow back into the sump when pumping has stopped. A small flow of nitrogen is maintained across the gas space above the sump to reduce air ingress, thus reducing corrosion. The MSTL gas system's major components are shown in the piping and instrumentation diagram (Fig. 6).

The dry nitrogen is supplied by a standard liquid nitrogen dewar utilizing the gas supply outlet. The dewar can supply up to 1480 kPa of gas, but this is regulated down to approximately 170 kPa. The pressure of the gas in the sump tank is approximately 136 kPa both when the pump is idle and when in operation. A scale is used to track the weight of the dewar so that a replacement can be ordered as the gas is used up. The gas flows from the dewar, across a Sensirion SHT15 humidity sensor, and into the gas distribution rack. Depending on the valve configuration, the gas can be sent to the vent at the top of the loop, to the sump tank, or to supply a sampling container with nitrogen. Exhaust from the sump tank is then routed back to the gas distribution rack, through a second humidity sensor, through a mineral oil gas bubbler, and out to the fume hood. The second humidity sensor allows tracking of the difference between humidity in the input nitrogen stream and the humidity present in the exhaust stream. This is important for monitoring and preventing corrosion, when drying the salt for an initial melt, or when adding salt to the system later. The mineral oil bubbler provides an easy way to ensure gas flow at a reasonable rate that can be monitored without electronic instrumentation. This flow rate is measured by a mass flow controller in the input line of the system after the regulator but before the gas distribution rack. Significant effort went into reducing this leakage, and the majority of the gas flows out through the shaft packing of the pump. The leakage can be slowed temporarily by tightening the packing, but as the pump operates, the leakage worsens quickly as the packing wears.

3.5. Trace heating

Trace heating of the loop is required to maintain salt temperature as pumping starts. Various lengths of commercially available 25 mm-wide fiberglass-insulated Ni-alloy heat tape are used to heat the loop. The trace heaters are rated for use at 240 V and up to 760 °C. Altogether, 3015 W (at 208 V) could be applied to the loop via trace heating. The trace heat was divided into two control channels with the south channel supplying up to 1140 W and the north channel supplying up to 1875 W. Without trace heating, the salt would freeze in the loop and cause a blockage. Additionally, trace heating the loop slowly to the salt melting temperature rather than flowing hot salt through the cold loop reduced mechanical stress in the system. The heat tape was wrapped around the pipes in a spiral manner. Great care was taken to ensure that the tape does not touch itself, causing a hot spot and subsequent failure. Additionally, aluminum foil was used to wrap around the heat tape to spread heat more evenly. The insulation (mentioned above) was installed over the aluminum foil layer.

3.6. Data acquisition and control

The data acquisition (DAQ) system was assembled to read out thermocouples, gas pressure transducers, a tachometer, salt flow meters, and humidity sensors, as well as control components including cover gas valves, flow controllers, heaters, and the salt pump motor. The system utilizes the Maximum Integrated Data Acquisition System (MIDAS) (Ritt and Amaudruz, 1997) software running on a main computer and various remote single board computers located near the instrumentation hardware. The main computer is used for user control and data storage. An Ethernet network connects this main computer to various DAQ hardware either directly, through media converters, or through various single board computers, as summarized in Fig. 7.
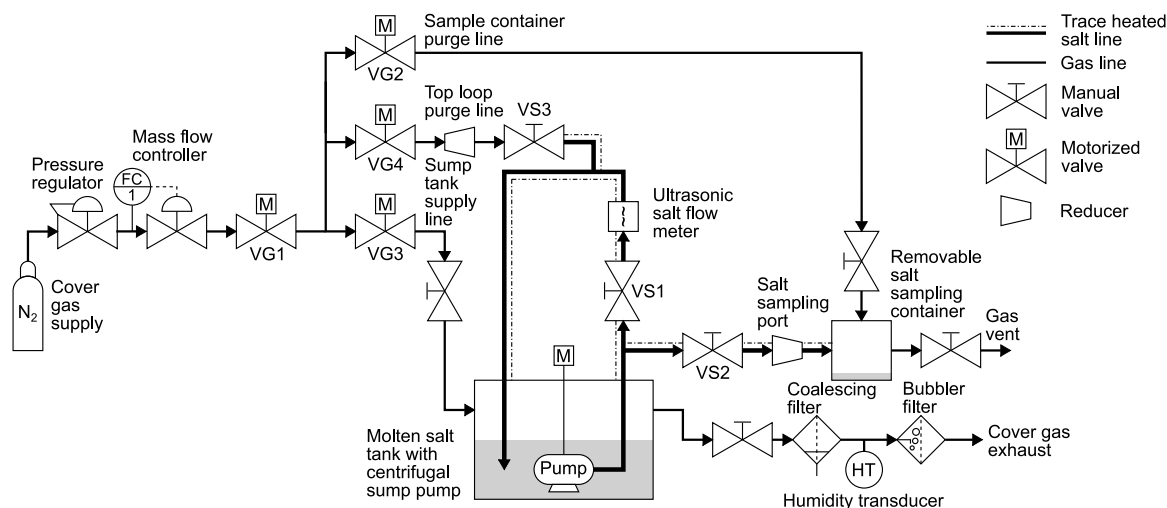
Fig. 6. Simplified piping and instrumentation diagram focusing on the cover gas system and molten salt loop.
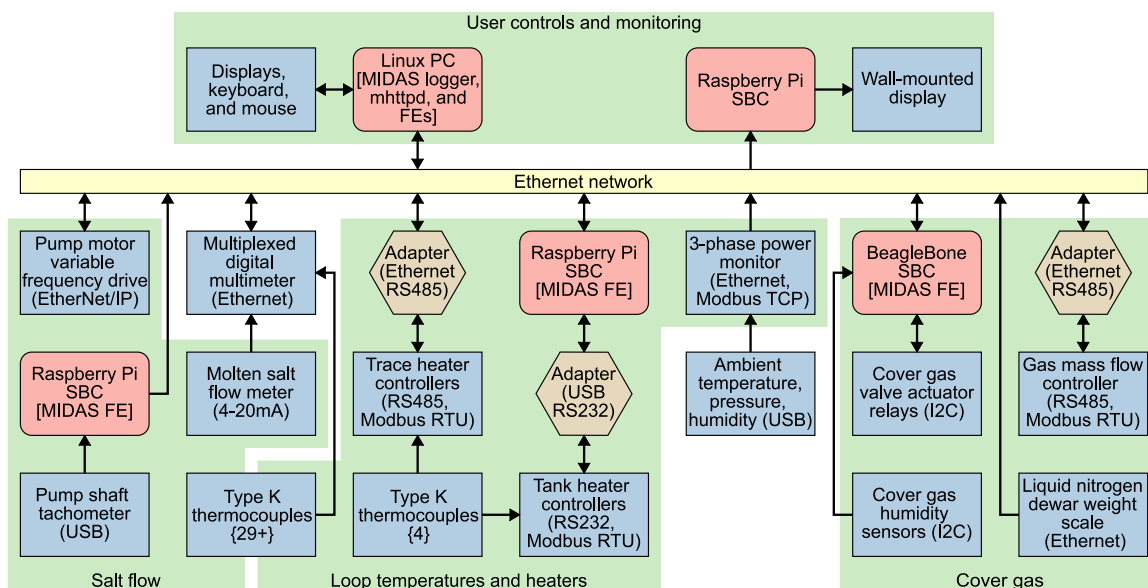

Fig. 7. An overview of major DAQ components. Solid lines summarize connections, data flow, and control directions (arrows). Communication protocols and signaling layers are in parentheses. Brackets include key software such as MIDAS frontend (FE) programs. Braces indicate the quantity of sensor channels.

The DAQ system includes MIDAS frontend programs written in C and C++ to support each piece of hardware. All of the frontends use the MIDAS slow controls driver framework. The MIDAS multimeter (multi.cxx) class driver and RS232 and TCP/IP bus drivers were used extensively. The MIDAS history system was used to archive most system data and for trend plotting.

Several instruments and readouts were used to monitor and ensure proper operation of the system at all times. This instrumentation includes two visible light cameras that give views of the system from different angles and can record video. The cameras can be set to record on movement, to record all the time, or to stream images. A thermal camera is used to monitor external system temperatures or to monitor heat trace elements. This is a very useful tool for identification of hot spots, but care must be taken as the IR can be reflected from the stainless steel components, giving false readings. Dedicated indicator lights set within the DAQ allow for red, green, or white indications. Red is used as an indication that the system is hot and caution should be taken, green when the system is cool, and white is currently unused. Additionally, two local monitors display the time and important system parameters, such as salt temperature and flow rate, so that they can easily be monitored by anyone in the room.

4. Pre-salt initialization and system tests

A suite of initial tests were completed on the MSTL systems to ensure the operation of the system and to collect enough data with a known fluid (water) to create a baseline that could be compared with both hydraulic theory and experimental data from flowing molten salt. These tests included taking flow and pressure measurements while varying the pump rotational speed at both room temperature and 90 °C; calibration of the Sotera water flow meter by measuring pumped water mass; and calibration of a Krohne Optisonic 4400HT flowmeter against the Sotera flow meter, testing both the salt sump heaters and the trace heaters and gas flow testing the gas blanket system.

4.1. Trace heater tests

Trace heaters were tested after all water tests were complete and the system was ready to be dried, but before salt was added to the system.
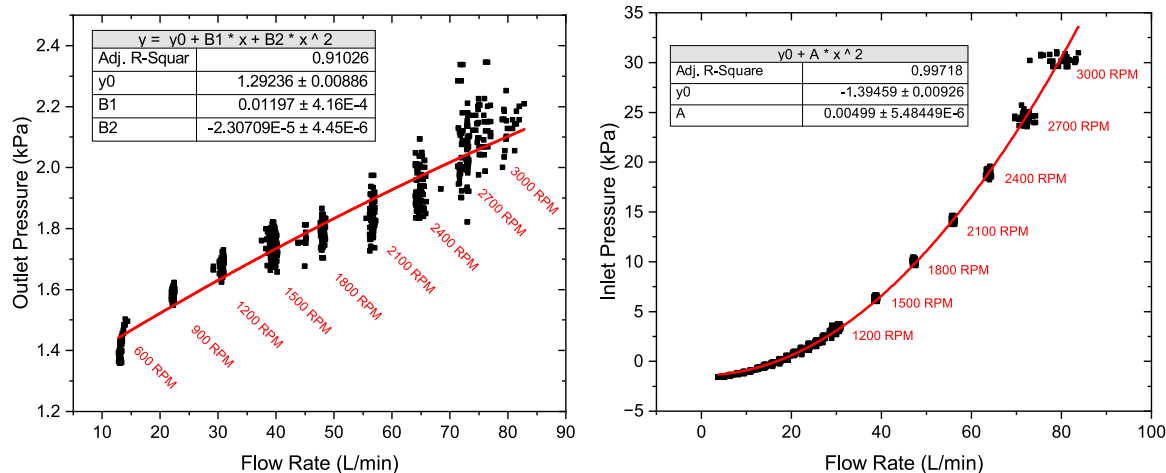
Fig. 8. Water pressure measured at inlet/outlet compared to flow rate measured by Krohne flow meter.

Type K thermocouples were mounted between the trace heaters and the pipe to provide temperature measurements and control of the trace heaters. Initial testing was just above room temperature and without insulation, and everything worked well. Subsequent testing at higher temperatures showed that the heat tape has a tendency to fail anywhere it crosses a fitting edge. Aluminum foil was used to smooth profiles around fittings so that heat could be more easily transferred away from the trace heaters. This was successful, and the trace heating was stable up to the maximum temperature of the system.

4.2. Testing the pump

Once the pump was reinstalled and the loop was assembled, but before running the MSTL with molten salt, shakedown testing with water was undertaken. During this suite of tests, leaks in the pipe joints were identified and repaired, a set of pressure transducers were installed on the discharge and return lines of the loop, two flow meters were installed, and a characteristic curve for the pipe system was produced.

The first flow meter was a Sotera model 825p nutating disk-type flowmeter, which has a maximum operating temperature of 54 °C. It was installed approximately 60 cm from the pump discharge. This instrument was only meant for use with water in initial testing and then later comparison with a flowmeter usable with low-temperature molten salts. Additionally, for calibration, the loop return was temporarily arranged in a way that allowed pumping water through the flow meter and into a large drum sitting on a scale in order to calibrate and verify the flow meter readings.

After the initial calibration of the Sotera flow meter, a Krohne Optisonic 4400 HT flow meter was installed upstream of the Sotera flow meter, which was moved to a position several feet farther around the loop. The Krohne flow meter has a maximum operating temperature of 400 °C, which is more than sufficient for molten nitrate salts. The Krohne flow meter calibration was then confirmed both by using the Sotera flow meter and measuring the water mass pumped into a drum.

A characteristic curve for the system was generated by simultaneously measuring the pressure at the inlet and outlet and the flow rate of water through the pipe. Unfortunately, one of the pressure transducers failed during these tests, so the pressure at the inlet and outlet were measured during separate runs. Combined, these measurements provide data on the pressure drop through the loop as a function of flow rate. These data and polynomial fits can be seen in Fig. 8. Pressure measurements in Fig. 8 had more scatter at higher pump rotation rates. This might be due to gas bubbles in the system at higher rotation rates. The data do show a clear trend between the pressure at the pump discharge or inlet to the loop and the rotation rate. A similar trend

is seen on the pressure at the outlet side of the loop, but the signal to noise level is significantly lower because the absolute pressure is lower there.

4.3. Testing the gas system

The gas system was tested piece by piece, then by pressurizing the system and flowing nitrogen through it before salt was introduced. The humidity sensors were compared to standard humidity sensors at room temperature before installation. Gas flow through the system was checked for each channel individually with enough gas pressure to ensure return through the bubbler.

4.4. Modifying the loop return level

The initial loop design discharged the liquid once it had flowed through the loop from the flange the pump is mounted on. This discharge traveled through the gas in the sump tank and splashed into the liquid there causing bubbles that were subsequently sucked into the system, which contributed to significant vibrations in the pump. The presence of bubbles was determined by temporarily replacing one of the steel loop pipe sections with a clear PVC section of pipe that allowed for observation of macroscopic bubbles flowing through the system. A remedy for this problem was moving the outlet of the liquid return from the pump mounting flange to beneath the sump liquid level and even with the top of the pump volute. This change eliminated the issues with bubble entrainment, and greatly reduced vibrations at most pump drive frequencies. The clear tubing was then removed and replaced with a stainless steel section. Pump vibrations were reduced further by re-balancing the impeller and the pump shaft.

Changing the loop return level introduced a new issue in the system: the loop would no longer drain. Because both the inlet and outlet of the loop are below the liquid level of the sump, liquid was trapped in the loop with no way to allow gas into the system. The problem was addressed by adding a tee and a valve to the high corner of the loop and connecting that to the gas blanket system, allowing gas to be added to the loop at a higher pressure than the pressure in the sump tank. This higher pressure gas overcomes the head pressure of the salt in the sump, forcing the salt out of the loop and into the sump. Because the pump discharge level is lower than the liquid return level, a salt-wetted valve in the loop is used to ensure that the liquid is evacuated from the entire loop. This is monitored by listening for gas bubbling through the liquid.
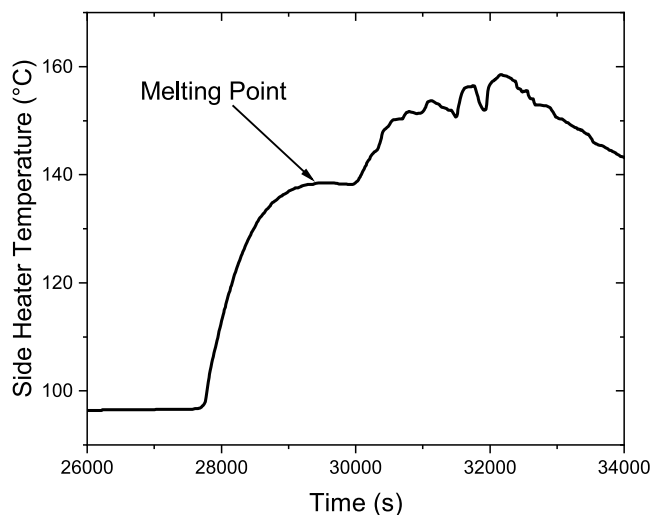
Fig. 9. Temperature of the thermowell in the salt as a function of time during the salt melt when heaters were on. The plateau at 138 °C indicates the salt melting temperature.

Fig. 10. Thermocouple values were a crucial tool to ensure molten salt flow around the loop. Preceding pump start, the thermocouples placed around the loop had a variety of temperatures, depending on their position with respect to trace heaters and varying heat losses. After the pump starts, the temperatures quickly converge to the single salt temperature, indicating that the salt is flowing through the entire system.

5. Operational modes and experiments

5.1. Salt loading and melting

When the MSTL was both dry and free of rust, the system was baked above 105 °C with dried compressed air running through the system until humidity sensors reached a low steady-state value. Once the system was dry, Dynalene MS-2 salt was loaded from the plastic buckets in which it came from the supplier into the MSTL through a funnel and an empty 1-inch open port in the pump flange (see Fig. 3).

Loading salt was difficult because the hygroscopicity of the salt caused it to stick to itself and the walls of the funnel. A metal pushrod was used to help clear the funnel opening when it clogged. Salt was loaded from two containers and added in two batches because there was not enough volume for the needed amount of salt in granular form. The second batch was added after the first batch melted. From the first container of salt, 13.65 kg was loaded into the sump tank. A further 7.21 kg was loaded from a second container for a total of 20.86 kg of salt in the system. It is unclear how much water was absorbed from the atmosphere in the transfer process. After salt loading, the humidity sensor on the output of the off-gas system did show 21 percentage points higher relative humidity than the sensor on the input side. After all of the salt was loaded, the heaters were set to 105 °C to aid in drying and left overnight with dry gas flowing across the system. The salt was melted by increasing the temperature of the heaters until it was clear that the salt was all at a temperature of at least 150 °C (see Fig. 9 for a typical melt). At that point, the salt was left at 150 °C overnight to ensure that all of the salt was in fact melted before pumping.

Before loading the salt into the system, samples of the salt were taken for chemical analysis and later comparisons. A 91.4 cm-long by 0.95 cm-diameter threaded rod was used as a molten salt sampling device. The rod could be held a long distance from the sampling end. Upon contact with the rod, the salt hardened immediately. The frozen salt sample was later removed by breaking it off of the threaded rod, which was relatively easy. Subsequent salt samples were acquired immediately after melting, on a regular basis for several weeks after the initial melt, and occasionally thereafter.

5.2. Salt circulation with the pump

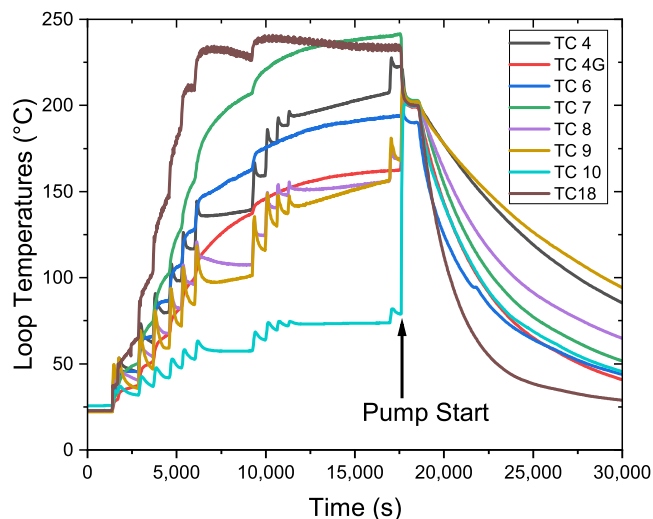Forced flow salt circulation was accomplished the day after the initial salt melt. The salt in the sump was heated to 180 °C. In preparation for the circulation, we performed two major system tasks. First, the pump was run at 1 Hz for a few seconds to ensure that the shaft turned freely as expected. Second, the loop was heated until the majority of thermocouples around the loop showed that they were at or above the salt melting point. Once the loop preheating was finished, and the vent valves (VS3 and VG4 in Fig. 6) at the top of the loop closed, the pump was started with the main salt-wetted valve (VS1) closed. The pump was ramped up to 55 Hz, and the valve was opened. Valve VS1 was left open as flow was started for subsequent runs. Flow was deduced by the convergence of the loop thermocouples to a consistent temperature (Fig. 10). Additionally, the heat lost to the loop was evident in cooling of the salt sump temperature (Fig. 11). After salt had flowed through the system for approximately 10–12 min, the team used the salt sampling port and valve to extract a sample of the salt into a container. Even the several centimeters of tube coming from the salt sampling valve (VS2 in Fig. 6) required trace heating to allow salt to flow through it.

After trying several different temperature and pump speed settings, the shutdown procedure was initiated. The pump was stopped, the vent valve (VS3 in Fig. 6) was opened, and pressurized dry nitrogen was inserted to allow salt to drain back into the sump tank. During this time, the valve VS1 (in Fig. 6) was closed for 1 min and then reopened. Bubbling could be heard as the gas came out of the loop piping, rose through the salt, and ended in the covergas space. Bubbling was confirmed with valve VS1 open and closed. Once the salt had drained from the loop, the trace heaters were turned off and the two sump heater zones reduced to 180 °C. This was chosen as a good temperature at which to leave the system unless there would be a long period of inactivity, in which case, all heaters would be turned off and the salt allowed to freeze. Because the salt for this system has a low melting temperature and the sump is well insulated, the natural cooling rate was used.

In addition to the use of thermocouples to observe the onset of salt flow, the Krohne flow meter was used to measure salt flow rate in the system. The flow meter was ultimately effective in monitoring the salt flow, but it was very sensitive to bubbles in the salt. Despite this sensitivity, a curve for flow rate vs pump rotation rate was developed and is shown in Fig. 12 to compare with data from water. This flow meter is acceptable for the Dynalene MS-2 salt but has a maximum operating temperature of 400 °C. Advanced reactors
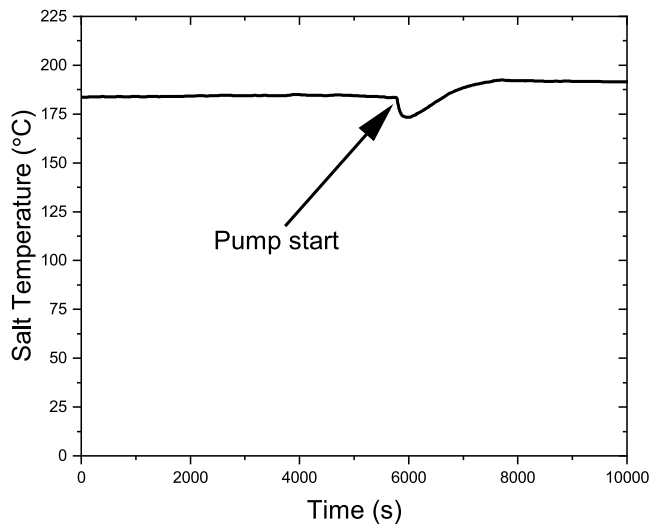
Fig. 11. Temperature of the salt in the MSTL sump tank. The dip near 6000 s occurred just as circulation of the salt through the loop began because the salt lost heat as the loop came to a steady state temperature, and the lower temperature of the salt is reflected by the dip shown here.
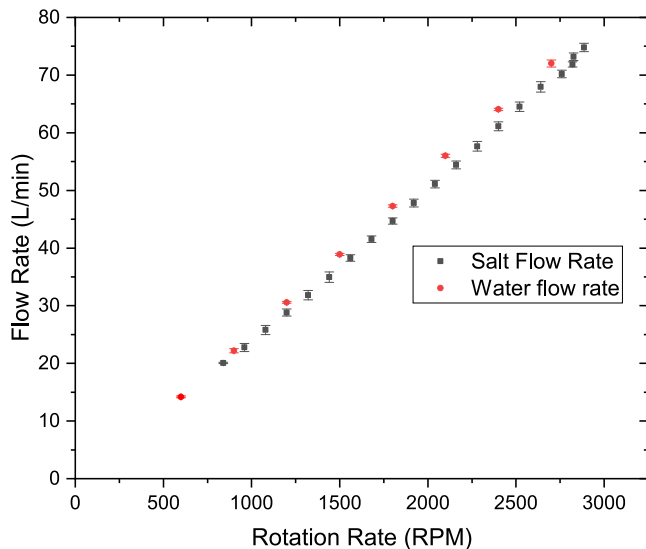

Fig. 12. Measured flow rates using the Krohne flow meter for water at room temperature and Dynalene MS-2 at 250 °C.

will likely need to maintain working temperatures in the 600–700 °C range. A flow meter for molten salt was not available for this temperature range. The team developed an alternative flow meter for higher temperature applications using ultrasonic transducers insulated by a calcium-silicate-based ceramic that could both insulate the transducers from the high-temperature pipe but also transmit ultrasound well enough to send and receive signals through the 25 mm diameter pipes (Head and Towell, 2020). Testing this device required a section of the piping to be flattened to increase the acoustic transmission area.

After freezing the salt the first time, the procedure for remelting ensures that the top zone of the sump heaters is well above the melting temperature of the salt and in fact that the majority of the salt is melted (as shown by the thermowell thermocouple readings) before the bottom heaters are used. This procedure prevents tank deformation or rupture that could occur if salt were melted at the bottom with no way to relieve pressure built up as it expands. Typically we have allowed the salt to freeze over long holidays when no one is around in case a power outage were to cause heater controller issues.
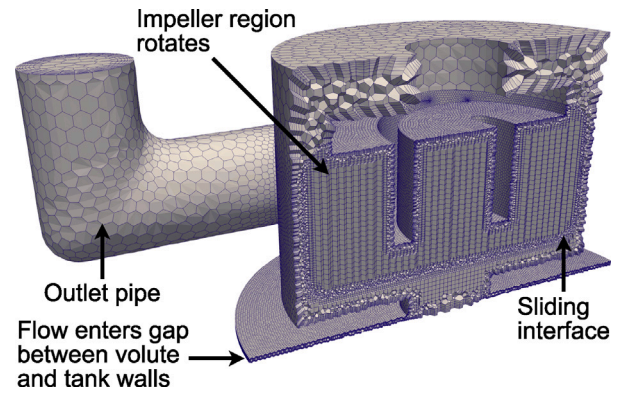

Fig. 13. Mesh of the pump with a 1.6 mm inlet gap, including the rotating impeller region and the stationary volute region. Connection of the two regions is accomplished through a sliding interface.

6. Computational fluid dynamics simulation

A series of simulations were performed to confirm the experimental results measured for water. These simulations provide a bridge for extrapolation to salt, for which several of the measurement techniques will no longer work due to the constraints of the high-temperature environment.

The pump's volute and spinning impeller were modeled in Ansys® Academic Research Fluent, release 2021R2 (Ansys Inc, 2021) to generate a pump curve. To accomplish this, simulations were run over a range of rotational speeds and volumetric flow rates, and the pressure difference between the inlet and outlet of the volute were compared.

Unfortunately, there was some uncertainty in the gap between the bottom of the volute and the tank. According to the design and computer-aided design modeling, the gap was approximately 1.6 mm. With that small of a gap, the inlet pressure is very sensitive to the precise value. For this reason, two models were simulated: one with the nominal 1.6 mm gap, and another with a 3.2 mm gap.

Both computational fluid dynamics (CFD) meshes were generated using Fluent Meshing (Ansys Inc, 2021) with a polyhedral-hexcore volumetric mesh. The 1.6 mm mesh had 1.2 million cells and 3.4 million nodes, and is shown in Fig. 13. The 3.2 mm gap mesh had 0.94 million cells and 2.9 million nodes. The difference in node count was primarily due to the higher refinement needed to mesh the narrower gap.

The pump was simulated as transient flow, with mesh motion applied on the impeller region. The impeller and volute regions were connected through a sliding interface. The boundary condition at the outlet was chosen to maintain a constant pressure of 0 Pa. At the inlet, a specified mass flow rate boundary condition was chosen, with the mass flow rate determined by the desired volumetric flow rate for the simulation. Moving wall boundaries were also applied for the shaft and portion of the impeller that was defined within the volute region.

Fig. 14 depicts the pressure in the pump as calculated from a CFD simulation of the pump run at 2800 RPM and a volumetric flow rate of 80 L/min. The lower pressure in the center of the impeller draws fluid through the inlet. The rotation of the impeller forces fluid to exit through the outlet pipe at higher pressure.

A transient simulation was performed and the evolution of the inlet pressure over time generated to determine the pressure provided by the impeller. The pressure is not constant as the impeller rotates, so an average value is taken over one full rotation. Fig. 15 provides the evolution of the inlet pressure for the pump with 1.6 mm gap run at 2800 RPM and a volumetric flow rate of 80 L/min.

The inlet pressure varies as the pump rotates, oscillating at twice the rate of the pump because of the two blades of the impeller.
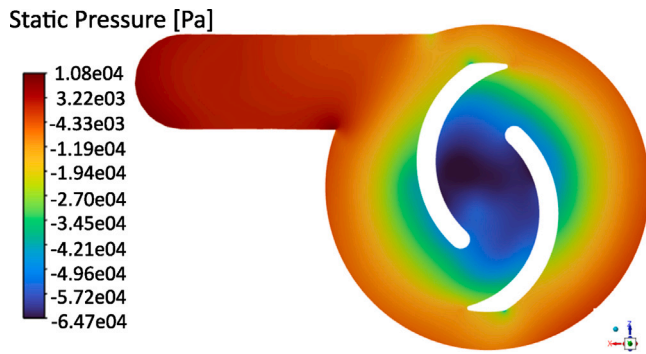
Static Pressure [Pa]

Fig. 14. Pressure distribution in a horizontal slice of the pump volute as it is run at 2800 RPM with a volumetric flow rate of 80 L/min. The slice bisects the outlet pipe.
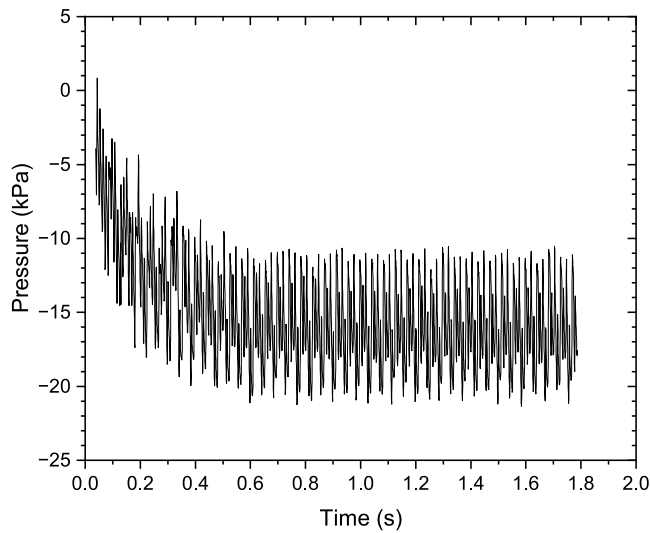

Fig. 15. Inlet pressure variation with time from transient simulation of the pump run at 2800 RPM with a volumetric flow rate of 80 L/min. Time zero is the start of the simulation.

However, after a few seconds of simulation, the oscillations vary only slightly between cycles, and an average value can be calculated. Once stabilized, the average inlet pressure is calculated over the remainder of the simulation.

By varying the volumetric flow rate and rotational speed, a family of pump curves can be generated. It is expected that the pump curves should follow turbomachinery scaling laws (Hibbeler and Yap, 2020) ($Q \propto \omega D^3$, $\Delta p \propto \omega^2 D^2$, where Q is the volumetric flow rate, ω is the rotation rate, p is pressure, and D is a characteristic length). Using these, all simulated data were scaled to a rotation rate of 1200 RPM. The result, along with a polynomial fit of the data, is shown in Fig. 16. The pump data for both gap sizes collapse well to parabolic fits.

A more general set of reduced parameters have been defined and compared to data from the specific system parameters. The reduced speed is defined as $\omega_R = \omega/\omega_0$, where ω is the rotation rate in RPM, and ω_0 is 1200 RPM. The reduced pressure is defined as $\Delta p_R = \Delta p/\Delta p_0 \omega_R^2$ where Δp is the pressure head across the pump in kPa, and Δp_0 is 11.417 kPa corresponding to the average pressure at zero flow at ω_0 for the two cases. Finally, the reduced flow rate is $Q_R = Q/Q_0 \omega_R$, where Q is the volumetric flow rate in L/min, and Q_0 is 175.65 L/min corresponding to the volume swept by an impeller blade turning at ω_0 for one second.

The pump speed and flow rate data were used to determine the pressure provided by the pump, based on the equation below:

$$\Delta p_R = 1 + B_1 Q_R + B_2 Q_R^2 \tag{1}$$

Table 1
Fit coefficients for scaled pump curves (Eq. (1)) to simulation results shown in Fig. 16.

Gap size (mm)	B_1 (−)	B_2 (−)
1.6	-0.5018 ± 0.2176	-18.751 ± 0.771
3.2	-0.2087 ± 0.12	-6.986 ± 0.424

The coefficients B_1 and B_2 are given in Table 1.

An empirical system curve was developed from the parabolic fit of pump data shown in Fig. 8 to compare the CFD predicted performance with the experimental results. For a large number of pump speeds, the flow rate was determined from experimental data (see Fig. 17).

The predicted pump pressure curves bracket the measured inlet pressure. The primary source of error is likely the measurement of the gap between the bottom of the pump inlet and the tank bottom. The measured value was 1.6 mm, which is much narrower than suggested by literature for optimal performance of 0.3–0.5 inlet diameters, or 7.5–12.5 mm in this case (American National Standard for Pump Intake Design 9.8-1998, 1998). The pressure loss due to friction is very sensitive to small changes in position, and the measured values indicate that the true gap width is between the two simulated widths, likely closer to 2.4 mm. Regardless, these simulations show the ability to provide good performance estimates for future pumps, especially if small gaps are avoided.

7. Salt properties measurements

Differential scanning calorimetry (DSC) was performed on samples taken from the loop to ensure that no higher-melting temperature species were formed during the circulation of nitrate salt. DSC scans that were performed on the nitrate salt prior to introducing the salt into the loop showed similar melting curves to samples removed from the loop, with the presence of slightly off-eutectic peaks in addition to the eutectic melting peak. In this case, the heterogeneity of the nitrate salt mix is maintained and evident from samples extracted from the loop, demonstrating that representative sampling can be performed on this system.

The Dynalene MS-2 samples were removed by diverting salt flow through a manually-operated valve and into a metal container. The molten salt was poured out onto a sheet of aluminum foil at room temperature and was allowed to freeze. Portions of the frozen salt were then broken off from either the center of the frozen salt sheet or near the edge. These samples were then placed in separate beakers and re-melted in an oven at 340 °C where they were stored for several days. The contents of a given beaker were then poured out onto a sheet of aluminum foil at room temperature, allowed to freeze, and homogenized with a mortar and pestle. The salt was transferred to a vacuum jar and kept under vacuum until a portion ranging between 6 and 10 mg was transferred to a 40 µL aluminum crucible that was sealed with an aluminum lid that had been punctured with a small hole. DSC scans were performed on the sample showing a melting point at approximately 123.0 ± 0.7 °C (Fig. 18). The melting point is defined by the point where a line tangent to the exothermic rise on the curve intersects with a line tangent to the curve before the transition.

Depending on the sample that was tested, the melting peak at 123 °C was followed by a second peak at 130.0 ± 0.1 °C, which was the result of off-eutectic ratios melting at higher temperatures. The ratio of the peak integrals varied according to the location of the salt sample taken from the larger frozen MSTL extraction. Samples taken near the edge of the frozen salt sheet showed an integral ratio of 0.9:1 (eutectic:off-eutectic) while samples from the center of the sheet showed an integral ratio of 0.7:1 (Fig. 19). A eutectic mix of $LiNO_3$-$NaNO_3$-KNO_3 (17-30-53 mol%) prepared in the lab showed a dominant eutectic peak with a smaller off-eutectic peak yielding an integral ratio of 1.4:1. For each
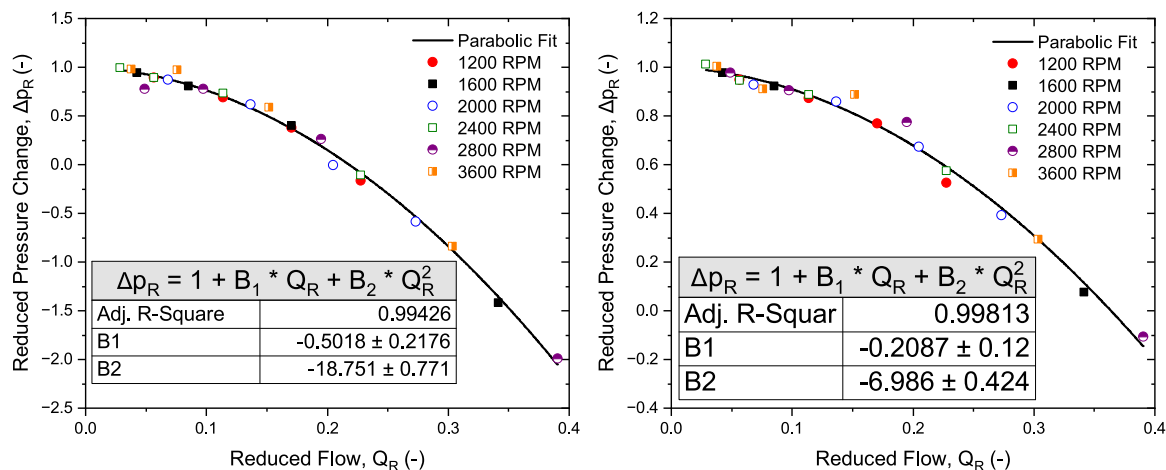
Fig. 16. Simulated pump curves with 1.6 mm gap (left) and 3.2 mm gap (right) scaled to 1200 RPM using turbomachinery scaling laws.
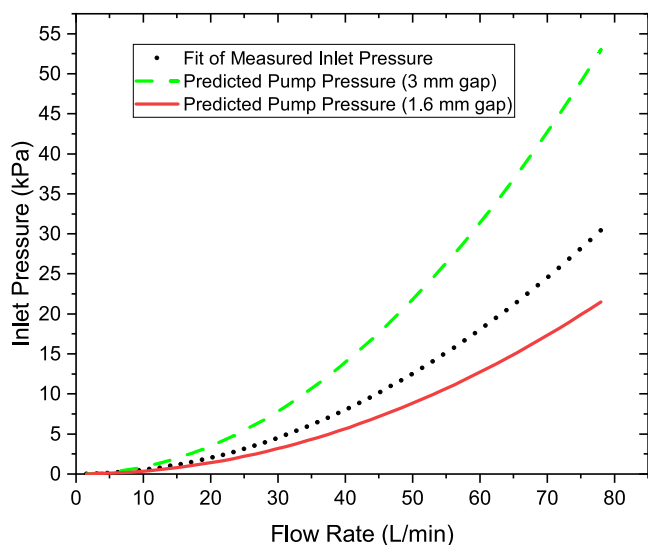

Fig. 17. Experimentally measured inlet pressure vs CFD-predicted pump pressure for a variety of pump speeds. For each pump speed, the experimentally determined flow rate was used to calculate the predicted pump pressure. CFD values were determined from the pump curves relationship shown in Fig. 16. The dotted curve is a fit to measured experimental data, the dashed line is predicted pressure for a 3.2 mm gap, and the solid line is predicted pressure for a 1.6 mm gap.
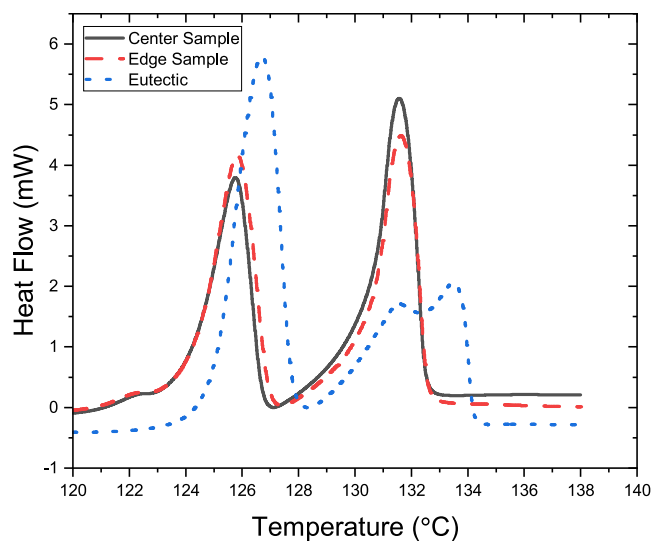

Fig. 18. DSC scans (endothermic up) of samples removed from the center of a frozen sheet of Dynalene MS-2 extracted from the MSTL, the edge of a frozen sheet of Dynalene MS-2 extracted from the MSTL, and of $LiNO_3$-$NaNO_3$-KNO_3 (17-30-53 mol%) prepared in-lab.

sample, a minimum of three temperature scans were performed at a rate of 1.0 °C/min.

DSC measurements of the Dynalene MS-2 salt demonstrate that there is inhomogeneity in both the overall chemical composition of the salt and as a function of sampling method. The DSC scans in Fig. 18 demonstrate that Dynalene MS-2 begins melting at about 123 °C, which is very close to the expected melting point of Li-Na-K-NO_3 eutectic. However, there are melting peaks that occur at temperatures above this initial peak, demonstrating that the composition of the Dynalene MS-2 is not at the eutectic ratio throughout. The relative amount of Dynalene MS-2 at the eutectic ratio versus an off-eutectic ratio can be measured by comparing the melting peak integrals of the lower (eutectic) and higher (off-eutectic) melting peaks. Fig. 19 demonstrates that depending on where the salt is sampled (from the edge or the center of a re-frozen sheet), the relative amount of eutectic-ratio and off-eutectic ratio salt will vary. Salt taken from the edge of a frozen sheet will have a higher surface-to-volume ratio than salt taken from the middle of the sheet. The difficulty in sampling exact eutectic mixes is demonstrated in the Li-Na-K-NO_3 eutectic mix prepared in-lab, which also displays an

off-eutectic melting peak. DSC samples typically consist of 5–10 mg of salt taken from grams of prepared sample. Sampling only the eutectic ratio becomes difficult unless extensive mixing/homogenization of the eutectic can be achieved or else the salt can be sampled as a liquid at the eutectic temperature.

8. Observations on operations

The original plan for this system was to upgrade it for use with a higher-temperature salt. We learned that the system had several issues that made operation at higher temperatures and with more corrosive salts impractical.

First, although the leakage of gas from the system was minimized to the point where it is affordable to maintain a positive nitrogen pressure in the system at all times, the leakage is still significant. Applications using fluoride salts or radioactive materials should utilize gas spaces with slightly negative pressures with respect to atmosphere so that harmful materials do not leave the system. A system where this is possible must have no leakage; otherwise, ingress of air into the system will cause corrosion. The major leak points identified in this system are
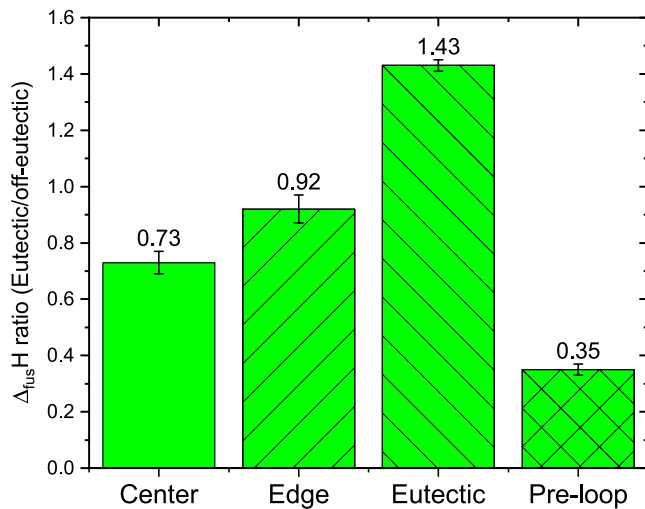
Fig. 19. Ratio of eutectic melting peak integral to off-eutectic melting peak integral (enthalpy of fusion) for Dynalene MS-2 sampled from the center and from the edge of a frozen sheet of Dynalene MS-2 pulled from the MSTL as well as a $LiNO_3$-$NaNO_3$-KNO_3 (17-30-53 mol%) eutectic mix prepared in the lab. A sample of Dynalene MS-2 was also taken from the salt container as-delivered and analyzed (pre-loop). Error bars represent standard deviation of at least three measurements.

the pump-shaft seal and the pump mounting flange seal. Everything else sealed reasonably.

The pump-shaft seal in this system is a simple packing seal that uses compression of a graphite-coated fiberglass rope against the pump shaft. The seal works reasonably well at first, but wears quickly. Also, a significant amount of motor torque goes into overcoming the friction of this seal, and it heats up quickly. Usage of a different type of shaft seal will be required for systems containing more highly corrosive salts.

The vibration issues with this long-shafted overhung pump without bearings in the salt are of potential concern and must be considered in reactor design where shielding may require pumps with significantly longer shafts. Shafts and impellers for these pumps will need to be precisely balanced and have large enough diameters to reduce vibrational modes over the range of pump rotation rates, or salt-wetted bearings developed.

The seal between the sump and the pump mounting flange also shows significant leakage. This seal began as a fiberglass rope seal sandwiched between the flat surface of the top of the sump and the flat bottom surface of the pump mounting flange but was later changed to a calcium silicate paper seal. While there was still some leakage, this reduced the level to something more moderate. Higher-temperature applications will likely need to employ large flanges with metal-to-metal seals for this purpose rather than trying to mate two flat surfaces.

The heater-pump system has a sump tank integrated into the heating box by welding the tank wall directly to the top plate of the heater. This is an issue for heat dissipation because of the direct connection between the high-temperature sump and the heater-box exterior. Reducing power consumption from this dissipation requires extra insulation. A higher-temperature system will need better thermal isolation of the sump tank from the exterior to reduce heating power as well as the hazards related to hot surfaces.

The MSTL used threaded pipe connections extensively. These connections had many issues with sealing and disconnecting and will not be viable in a system for higher temperatures where leakage is critical or where joints need to be repeatedly connected and disconnected. Although an attempt was made to seal the system without using PTFE tape, most of the threaded joints required some to seal. This limited the maximum temperature of the loop to 300 °C as the melting temperature of the PTFE is 327 °C (Christakopoulos et al., 2020). Additionally, after heating the system, galling of the threads became a significant issue in cases where it was necessary to take a joint apart. Higher-temperature systems will need to either omit joints altogether or use a flange made specifically for molten salt to avoid these problems.

Finally, addition of *dry* salt to the system through a 25 mm diameter inlet pipe using a funnel through the air was difficult and allowed the salt to absorb a significant amount of water during loading. A more corrosive or hazardous salt will need to be loaded into the system as a liquid transferred without contact with the air to minimize risk to people and reduce opportunities for ingress of water and oxygen into the system.

9. Conclusions

A molten salt test loop was designed, built, and commissioned to advance the technical readiness level of molten salt components and instruments in the NEXT Lab on the ACU campus. This system provided for the forced circulation of a molten nitrate salt through several meters of stainless steel 25 mm diameter pipe. An integrated data acquisition, monitoring, and controls subsystem and a dry nitrogen gas blanket subsystem were developed to support the MSTL. This complete system has supported the testing of a high temperature flow meter, CFD studies of flowing molten salt, and procedure development for salt sampling and measurement to better understand salt chemistry evolution. The advances in molten salt components and instruments made possible by the MSTL have informed plans for future gas-tight, high-temperature salt systems and paved the way for commercial applications of molten salts, including advanced reactors.

CRediT authorship contribution statement

T.L. Head: Conceptualization, Methodology, Validation, Formal analysis, Investigation, Resources, Data curation, Writing – original draft, Writing – review & editing, Visualization, Supervision, Project administration. **Allison M. Berry:** Writing – original draft, Writing – review & editing. **Keaton J. Brewster:** Design and fabrication, Software. **Robert L. Brown:** Formal analysis, Investigation, Data curation, Writing – original draft, Writing – review & editing, Visualization. **Hailey N. Burden:** Conceptualization, Formal analysis, Investigation. **Reuben Byrd:** Conceptualization, Methodology, Design and fabrication, Investigation. **Timothy Doty:** Investigation. **Jess Dowdy:** Design and fabrication, Investigation, Supervision, Project administration. **Kameron A. Hill:** Conceptualization, Investigation. **R.A. Jinkerson:** Conceptualization, Methodology, Design and fabrication, Writing – review & editing, Supervision. **Timothy J. Kennedy:** Methodology Design and fabrication, Validation, Investigation. **Ronald C. Laehn:** Conceptualization, Validation, Formal analysis, Investigation, Writing – review & editing, Visualization. **Dakotah Martinez:** Conceptualization, Formal analysis, Investigation. **Samuel L. Mulder:** Design and fabrication, Investigation. **Charles Onstead:** Design and fabrication, Investigation. **Kim L. Pamplin:** Conceptualization, Methodology, Validation, Formal analysis, Investigation, Writing – review & editing, Supervision. **Dylan C. Pfeifer:** Software. **Michael B. Ranger:** Methodology, Design and fabrication, Software, Validation, Formal analysis, Investigation. **Aaron D. Robison:** Investigation, Writing – original draft, Writing – review & editing. **Nathaniel T. Rowlands:** Validation, Formal analysis. **Raymond E. Smith:** Design and fabrication, Resources. **Matthew T. Steele:** Design and fabrication. **R.S. Towell:** Conceptualization, Methodology, Resources, Writing – original draft, Writing – review & editing, Supervision, Project administration, Funding acquisition. **Travis Towell:** Design and fabrication, Software. **Olive Tuyishimire:** Conceptualization, Methodology, Design and fabrication, Investigation, Writing – review & editing, Visualization. **T.S. Watson:** Design and fabrication, Software, Investigation, Data curation, Writing – original draft, Writing – review & editing, Visualization.

Declaration of competing interest

The authors declare the following financial interests/personal relationships which may be considered as potential competing interests: T. L. Head reports financial support for the project was provided by Natura Resources, LLC. T. L. Head reports a relationship with Natura Resources, LLC. that includes: funding grants. T. L. Head reports a patent for Apparatus Systems and Methods for Non-invasive Measurement of Flow in High Temperature Pipe (US patent 10,876,871).

Kim L. Pamplin has patent IDENTIFYING AND QUANTIFYING COMPONENTS IN A HIGH-MELTING-POINT LIQUID pending to Abilene Christian University.

Data availability

Data will be made available on request.

Acknowledgments

References

American National Standard for Pump Intake Design 9.8-1998, 1998. Standard Hydraulic Institute, Parsippany, NJ, USA.

Ansys Inc, 2021. Ansys® Academic Research Fluent. URL https://www.ansys.com/products/fluids/ansys-fluent.

Arora, O., Lancaster, B., Yang, S.R., Vaghetto, R., Hassan, Y., 2021. Advanced flow and temperature measurements in a forced convection molten salt test loop. Ann. Nucl. Energy 159, 108269.

Britsch, K., Anderson, M., Brooks, P., Sridharan, K., 2019. Natural circulation flibe loop overview. Int. J. Heat Mass Transfer 134, 970–983. http://dx.doi.org/10.1016/j.ijheatmasstransfer.2018.12.180, URL https://www.sciencedirect.com/science/article/pii/S0017931018346209.

Christakopoulos, F., Troisi, E., Tervoort, T.A., 2020. Melting kinetics of nascent poly(tetrafluoroethylene) powder. Polymers 12 (4), http://dx.doi.org/10.3390/polym12040791, URL https://www.mdpi.com/2073-4360/12/4/791.

2020. Dynalene MS-2 SDS. Dynalene, Inc.

Engel, J.R., Grimes, W.R., Rhoades, W.A., Dearing, J.F., 1978. Molten-salt reactors for efficient nuclear fuel utilization without plutonium separation. Tech. rep., Oak Ridge National Laboratory, http://dx.doi.org/10.2172/6650305, URL https://www.osti.gov/biblio/6650305.

Forsberg, C.W., 2006. Molten-salt-reactor technology gaps. In: Proc. 2006 International Congress on Advances in Nuclear Power Plants (ICAPP'06). Citeseer, pp. 4–8.

Forsberg, C.W., Renault, C., Le Brun, C., Ignatiev, V., 2007. Liquid salt applications and molten salt reactors. Rev. Géner. Nucl. 4, 63.

Gill, D., Kolb, W., Briggs, R., 2014. An evaluation of pressure measurement technology and operating performance using sandia's molten salt test loop. Energy Procedia 49, 800–809. http://dx.doi.org/10.1016/j.egypro.2014.03.087.

Head, T.L., Towell, R., 2020. Apparatus, systems, and methods for non-invasive measurement of flow in a high temperature pipe. US10876871.

Hibbeler, R., Yap, K., 2020. Fluid Mechanics in SI Units. Pearson Education, Limited, URL https://books.google.com/books?id=phROswEACAAJ.

Ho, M., Obbard, E., Burr, P.A., Yeoh, G., 2019. A review on the development of nuclear power reactors. Energy Procedia 160, 459–466. http://dx.doi.org/10.1016/j.egypro.2019.02.193, URL https://www.sciencedirect.com/science/article/pii/S1876610219312834. 2nd International Conference on Energy and Power, ICEP2018, 13–15 December 2018, Sydney, Australia.

Jeong, Y.S., Seo, S.B., Bang, I.C., 2018. Natural convection heat transfer characteristics of molten salt with internal heat generation. Int. J. Therm. Sci. 129, 181–192. http://dx.doi.org/10.1016/j.ijthermalsci.2018.01.036, URL https://www.sciencedirect.com/science/article/pii/S1290072917316599.

Jerden, J., 2019. Molten Salt Thermophysical Properties Database Development: 2019 Update. Tech. rep., Argonne National Laboratory, http://dx.doi.org/10.2172/1559846, URL https://www.osti.gov/biblio/1559846.

Kelleher, B.C., Gagnon, S.F., Mitchell, I.G., 2022. Thermal gradient mass transport corrosion in nacl-MgCl2 and MgCl2-nacl-KCl molten salts. Mater. Today Commun. 33, 104358. http://dx.doi.org/10.1016/j.mtcomm.2022.104358, URL https://www.sciencedirect.com/science/article/pii/S2352492822011990.

Kratochwil, C., Bruchertseifer, F., Rathke, H., Bronzel, M., Apostolidis, C., Weichert, W., Haberkorn, U., Giesel, F.L., Morgenstern, A., 2017. Targeted α-therapy of metastatic castration-resistant prostate cancer with 225ac-PSMA-617: Dosimetry estimate and empiric dose finding. J. Nucl. Med. 58 (10), 1624–1631. http://dx.doi.org/10.2967/jnumed.117.191395, arXiv:https://jnm.snmjournals.org/content/58/10/1624.full.pdf. URL https://jnm.snmjournals.org/content/58/10/1624.

Ludwig, D., Olson, L., Sridharan, K., Anderson, M., Allen, T., 2011. High temperature electrochemistry of molten fluoride salt for measurement of dissolved chromium. Corros. Eng., Sci. Technol. 46 (4), 360–364. http://dx.doi.org/10.1179/147842209X12579401586645, arXiv:https://doi.org/10.1179/147842209X12579401586645.

MacPherson, H.G., 1985. The molten salt reactor adventure. Nucl. Sci. Eng. 90 (4), 374–380. http://dx.doi.org/10.13182/NSE90-374, arXiv:https://doi.org/10.13182/NSE90-374.

None, N., 1972. Evaluation of the Molten Salt Breeder Reactor. Tech. rep., USAEC Division of Reactor Development and Technology, http://dx.doi.org/10.2172/4372873, URL https://www.osti.gov/biblio/4372873.

Ritt, S., Amaudruz, P., 1997. The MIDAS data acquisition system. In: Proc. IEEE 10th Real Time Conf. pp. 309–312.

Robb, K.R., Mulligan, P.L., Yoder Jr., G.L., Smith, K., Massengale, J., 2019. Facility to Alleviate Salt Technology Risks (FASTR): Preliminary Design Report with Failure Modes and Effects Analysis. Tech. rep., Oak Ridge National Laboratory, http://dx.doi.org/10.2172/1615802, URL https://www.osti.gov/biblio/1615802.

Rosenthal, M.W., Kasten, P.R., Briggs, R.B., 1970. Molten-salt reactors—History, status, and potential. Nucl. Appl. Technol. 8, 107–117. http://dx.doi.org/10.13182/NT70-A28619, arXiv:https://doi.org/10.13182/NT70-A28619.

Sabharwall, P., Ebner, M., Sohal, M., Sharpe, P., Group, T.H., 2010. Molten Salts for High Temperature Reactors: University of Wisconsin Molten Salt Corrosion and Flow Loop Experiments – Issues Identified and Path Forward. Tech. rep., Idaho National Laboratory, http://dx.doi.org/10.2172/980798, URL https://www.osti.gov/biblio/980798.

Sohal, M.S., Sabharwall, P., Calderoni, P., Wertsching, A.K., Grover, S.B., 2010. Conceptual Design of Forced Convection Molten Salt Heat Transfer Testing Loop. Tech. rep., Idaho National Laboratory, http://dx.doi.org/10.2172/1000546, URL https://www.osti.gov/biblio/1000546.

Stoddard, M., Harb, J., Memmott, M., 2019. Numerical analysis of isotope production in molten salt reactors: A case study for molybdenum-99 production. Ann. Nucl. Energy 129, 56–61. http://dx.doi.org/10.1016/j.anucene.2019.01.021, URL https://www.sciencedirect.com/science/article/pii/S0306454919300283.

Towell, R.S., 2018. URL https://acunextlab.org/.

Williams, D.F., Toth, L.M., Clarno, K.T., 2006. Assessment of Candidate Molten Salt Coolants for the Advanced High Temperature Reactor (AHTR). Tech. Rep. ORNL/TM-2006/12, Oak Ridge National Laboratory.

Worrall, A., Betzler, B.R., Flanagan, G., Holcomb, D.E., Hu, J., Kovacic, D.N., Qualls, A.L., Worrall, L.G., 2018. Molten Salt Reactors and Associated Safeguards Challenges and Opportunities. Tech. rep., IAEA.

Yoder Jr., G.L., Aaron, A., Cunningham, B., Fugate, D., Holcomb, D., Kisner, R., Peretz, F., Robb, K., Wilgen, J., Wilson, D., 2014. An experimental test facility to support development of the fluoride-salt-cooled high-temperature reactor. Ann. Nucl. Energy 64, 511–517.

Zhang, D., Liu, L., Liu, M., Xu, R., Gong, C., Zhang, J., Wang, C., Qiu, S., Su, G., 2018. Review of conceptual design and fundamental research of molten salt reactors in China. Int. J. Energy Res. 42 (5), 1834–1848. http://dx.doi.org/10.1002/er.3979, arXiv:https://onlinelibrary.wiley.com/doi/pdf/10.1002/er.3979. URL https://onlinelibrary.wiley.com/doi/abs/10.1002/er.3979.

Zheng, G., Wu, H., Wang, J., Chen, S., Zhang, Y., 2018. Thorium-based molten salt SMR as the nuclear technology pathway from a market-oriented perspective. Ann. Nucl. Energy 116, 177–186. http://dx.doi.org/10.1016/j.anucene.2018.02.004, URL https://www.sciencedirect.com/science/article/pii/S0306454918300586.